

# Investigation of the effectiveness of tandem oil fences under currents

CHOUNG MOOK LEE<sup>1</sup>, DONG GI HAN<sup>2</sup>, KWAN HYOUNG KANG<sup>1</sup>, and SANG JOON LEE<sup>1</sup>

<sup>1</sup>Department of Mechanical Engineering, Pohang University of Science and Technology, Pohang 780-784, Korea

<sup>2</sup>Applied Technology Research Department, Hyundai Mobis, Yong In 449-910, Korea

**Abstract** The behavior of the flow passing a tandem oil fence, and the performance of the fence, were investigated by experimental and numerical methods. The flow characteristics between tandem fences were measured by the particle image velocimetry (PIV) method for the rigid and open free surface between the two fences in order to gather reference data for numerical investigations. A method of assessing a tandem fence by tracing the movement of an oil droplet around the fence is introduced. The effect of the current speed, the separation distance between the two fences, the relative draft of the two fences, and the water depth on the oil containment between the fences was investigated.

**Key words** Oil spill · Tandem oil fence · Containment and recovery · Leakage velocity

## 1 Introduction

Once an oil-spill occurs in a coastal region, the only available physical device to prevent the oil spreading has been an oil fence. Unfortunately, it is well known that the effectiveness of an oil fence deteriorates rapidly once the current speed and wave height exceed certain limits. However, there are certain coastal territories which need contaminant-free water, such as fish farms, cooling water intakes for nuclear power plants, ecologically sensitive areas, and beach resorts. The chemical dispersants used to break up the oil patches may not be acceptable for such areas.

The concept of a tandem fence was thus initiated with the aim of developing a better device to safeguard those areas which must not be exposed to oil contamination. Several investigators have reported their results on the performance of tandem fences.<sup>1-4</sup> We have investigated

various hydrodynamic aspects of oil fences, both single and tandem.<sup>5-9</sup> This work is the result of investigations to assess the effectiveness of tandem oil fences which are subject to a uniform current.

The essence of a tandem oil fence lies in the fact that if the fore fence fails to contain the oil slicks, then the aft fence comes into a play to trap the leaked oil slicks between the two fences. Hence, the main focus of the investigation is on the flow behavior in the confined water region between the two fences. To analyze the flow characteristics in this region, a PIV method was used to obtain the flow velocity field in detail. In order to investigate the effect of the free surface, the experiment was performed with an open and a closed free surface. The velocity-field data thus obtained was sent to numerical investigators so that they could check the validity of their numerical results for the flow between two finite-depth vertical walls subject to a uniform current.

The assessment method for the effectiveness of a tandem oil fence is based on the Lagrangian particle-tracking method for an oil droplet which starts its motion up-stream of the fore fence. The water region ahead of the forward fence is defined as region 1 (R1), the region between the fences as region 2 (R2), and the region aft of the rear fence as region 3 (R3). Particle tracking checks the region where an oil droplet released at a known point in R1 would end up. If the droplet ends up in R1 or R2, the tandem fence is assessed as being effective.

This investigation was carried out by experiments using a circulating water channel, and by numerical computations using a Navier–Stokes solver. The assessment of the effectiveness of a tandem fence to contain the oil was performed using a flow-field computation and Lagrangian tracking of an oil droplet. Laboratory experiments were performed to check the validity of the numerical results. The assessment takes into account the effect of the current speed, the relative size of the

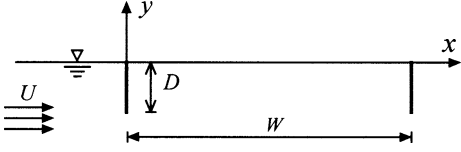


**Fig. 1.** Schematic diagram of the experimental set-up and coordinate system

two fences, the separation distance between the fences, and the ratio of the fence draft to the water depth.

## 2 Formulations

### 2.1 Flow field

We used the right-handed Cartesian coordinate system shown in Fig. 1. The two-dimensional fluid field in the presence of a set of infinitely long tandem fences was assumed to be steady, viscous, and incompressible, which is represented by

$$\nabla \cdot \mathbf{u} = 0 \quad (1)$$

$$\mathbf{u} \cdot \nabla \mathbf{u} = -\frac{\nabla p}{\rho} + (\nu + \nu_t) \nabla^2 \mathbf{u} \quad (2)$$

where  $\mathbf{u}$  is the fluid velocity,  $\rho$  is the density of water,  $p$  is the pressure, and  $\nu$  and  $\nu_t$  are the kinematic viscosity of laminar and turbulent flow, respectively. For a given free stream velocity  $U$ , the fluid boundaries are the free surface, the two rigid fences, and the surface at the bottom of the water. A no-slip condition is imposed on the latter two boundary surfaces, and a vanishing normal velocity condition is imposed on the free surface, i.e., the free surface remains flat.

### 2.2 Lagrangian particle tracking

Once the flow velocity field is known, the motion of an oil droplet of diameter  $d_e$  can be found by solving the following equation of motion given by Maxey and Riley<sup>10</sup> and Berlemont et al.<sup>11</sup>

$$\rho_o \frac{d\mathbf{u}_d}{dt} = -\rho C_A \frac{d\mathbf{u}_r}{dt} - \frac{\rho}{2} C_D \frac{A_e}{V} |\mathbf{u}_r| \mathbf{u}_r + (\rho_o - \rho) \mathbf{g} + \rho \frac{D\mathbf{u}}{Dt} \quad (3)$$

where  $\rho_o$  is the density of oil,  $\mathbf{u}_d$  is the droplet velocity,  $C_A$  is the added-mass coefficient normalized by the droplet volume  $V$ ,  $\mathbf{u}_r (= \mathbf{u}_d - \mathbf{u})$  is the velocity of the droplet relative to the fluid velocity,  $C_D$  is the drag coefficient normalized by  $\rho |\mathbf{u}_r|^2$ ,  $A_e$ ,  $A_e (\pi d_e^2/4)$  is the equivalent cross-sectional area of the droplet,  $d_e$  is the equivalent diameter of the droplet,  $\mathbf{g} = (0, -g)$  is the gravitational acceleration, and  $D/Dt$  is the substantial

time derivative. The coefficients  $C_A$  and  $C_D$  are obtained by the formulae given by Clift et al.<sup>12</sup>

## 3 Numerical method

The Navier–Stokes equations are solved by the finite-difference scheme with body-fitted grids, the standard  $k$ - $\epsilon$  turbulence model of Jones and Launder,<sup>13</sup> and a SIMPLE C algorithm for the velocity–pressure correction to satisfy the continuity of Eq. 1. The computation domain is  $x = [-15D, 25D]$ , and  $y = [-15D, 0]$ . The boundary conditions for steady and viscous flow are

$$\mathbf{u} = (U, 0) \quad \text{at } x = -15D \quad (4a)$$

$$\frac{\partial \mathbf{u}}{\partial x} = (0, 0) \quad \text{at } x = 25D \quad (4b)$$

$$v = 0 \quad \text{at } y = 0 \quad (4c)$$

$$v = 0 \quad \text{at } y = -15D \quad (4d)$$

where  $D$  is the fence draft. The exact free-surface condition is that the free surface should be treated as a material surface which allows deformation. However, in this work, since the uniform current velocity considered lies in the lower range, the rigid-wall condition of  $v = 0$  is assumed.

Equation 3 can be converted into a nondimensional form as

$$\rho_o \frac{d\mathbf{u}_d}{dt} = -C_A \frac{d\mathbf{u}_r}{dt} - \frac{3}{4} \frac{C_D}{d_e} |\mathbf{u}_r| \mathbf{u}_r + \frac{\mathbf{j}(\rho_o - 1)}{Fr^2} + \frac{D\mathbf{u}}{Dt} \quad (5)$$

where the normalizing quantities of  $\rho$ ,  $U$ ,  $D$ , and  $D/U$  for the density, velocity, length, and time, respectively, are used,  $\mathbf{j}$  is the unit vector in the  $y$ -direction, and  $Fr = U/\sqrt{gD}$ .

The integration of the equation of motion for an oil droplet given by Eq. 5 is carried out by using the fourth-order Runge–Kutta method. Once  $\mathbf{u}_d$  has been obtained, the position vector  $\mathbf{r}_d$  can be found by time-integration.

## 4 Experimental method

### 4.1 Experimental facilities and procedures

The experiment for the particle image velocimetry (PIV) measurement was carried out at a circulating water channel of which the test section size was 300 mm<sup>w</sup> × 200 mm<sup>h</sup> × 1200 mm<sup>l</sup>. A schematic diagram of the fence model and coordinate system used in this work is shown in Fig. 1. The draft ( $D$ ) and the separation distance ( $W$ ) of the oil fences are 40 mm and 320 mm, respectively, and the fence model has a flat tip

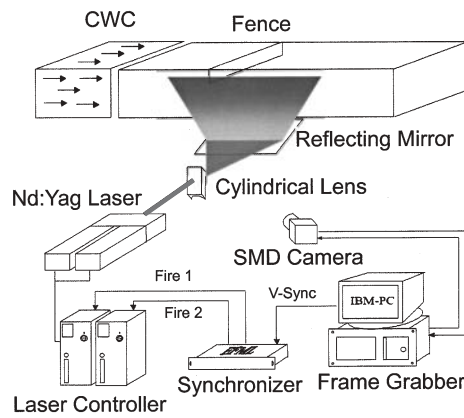


**Fig. 2.** Schematic diagram of the particle image velocimetry (PIV) velocity field measurement system

with a thickness ( $B$ ) of 5 mm made of acrylic material. The fence model was installed 400 mm down-stream of the test section. The free stream velocity was uniform at 10 cm/s, and its corresponding Reynolds number ( $Re$ ) and Froude number ( $Fr$ ) based on the fence draft were about 4000 and 0.16, respectively. The free stream turbulence intensity was about 0.5% at this velocity.

#### 4.2 Single-frame PIV system

The instantaneous velocity fields of flow around the oil fences were measured using a single-frame cross-correlation PIV technique. The PIV system is composed of a digital CCD camera, a two-head Nd:Yag laser, a synchronizing device, and an IBM PC with a frame-grabber, as shown in Fig. 2. A high-resolution CCD camera (SMD 4M4) was used to capture particle images with a  $2K \times 2K$  pixels resolution.

The basic procedure of the single-frame PIV technique is to capture a double-exposure particle image using the high-resolution CCD camera, and determine the particle displacement vectors during the time-interval  $\Delta t$  by calculating cross-correlation coefficients of the double-exposed particle image at each interrogation window. More details about the PIV method used in this investigation are given by Shin et al.<sup>14</sup>

#### 4.3 Droplet tracking

An experiment to obtain the trajectories of paraffin balls (Laboratory experiments using a paraffin ball and an equivalent diameter oil droplet were conducted by Lee et al.,<sup>7</sup> and it was found that they exhibited the same trajectories.) of density  $900 \text{ kg/m}^3$  and different sizes, which were released up-stream of a model fence, was carried out in a larger circulation water channel of  $1 \text{ m}^w \times 8.003 \text{ m}^h \times 4.2 \text{ m}^l$  in order to increase the Reynolds number to the order of  $10^4 \sim 10^5$  and make the balls

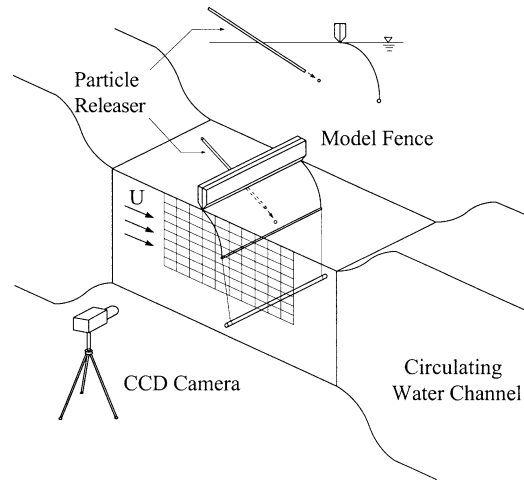


**Fig. 3.** Experimental set-up for measuring the trajectory of paraffin balls

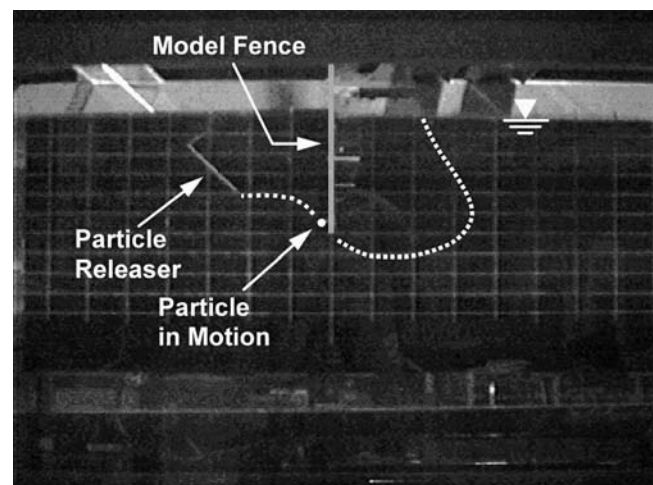


**Fig. 4.** Photograph of the trajectory of a paraffin ball

escape beneath the fence, which cannot be done in the smaller channel. The fence draft was increased to 150 mm and the Froude number to 0.292. Tracking the motion of the balls was done by CCD camera, as shown schematically in Fig. 3, and a sample photograph of the trajectory is shown in Fig. 4. As shown in Fig. 4, a small tube of 1 cm diameter containing a paraffin ball is inserted into the fluid to the desired release point, and the ball is then pushed into the water by a stick inserted into the tube.

## 5 Results and discussions

### 5.1 Velocity field

Figure 5 shows the flow velocity vector field for a single fence (case I), a tandem fence with an open free surface

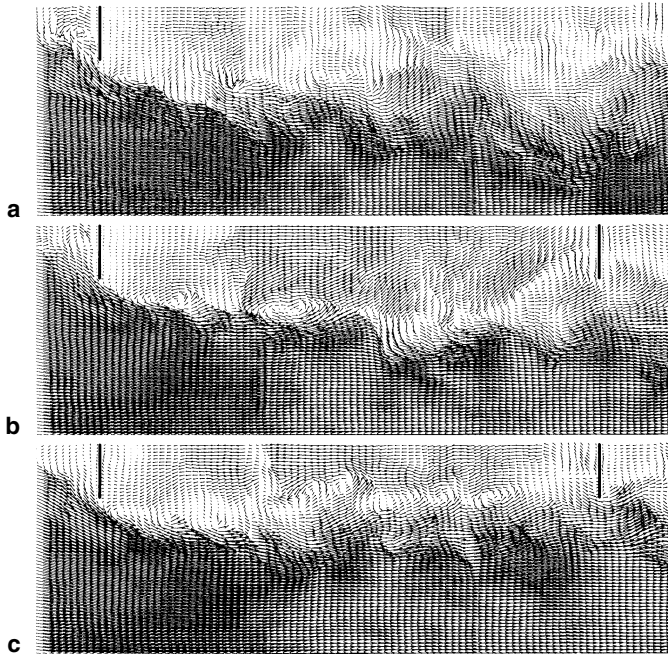


**Fig. 5.** Flow velocity field around single and tandem fences at  $Fr = 0.16$  and a fence separation distance of  $8D$  for the tandem fence: **a** Single fence with an open free surface. **b** Tandem fence with an open free surface. **c** Tandem fence with a closed free surface

(case II), and a tandem fence with a closed free surface (case III) at a Froude number ( $Fr = U/\sqrt{gD}$ ) of 0.16, and a fence separation distance for the tandem fence of  $8D$ . The velocity fields were obtained using the PIV method. Among the various combinations of fence separation distances and Froude numbers, this article presents the results of a fence separation of  $8D$  and a Froude number of 0.16, which correspond to a current speed of 1 knot ( $= 0.51$  m/s) and a fence draft of 1 m. The choice was based on in-situ reports of oil recovery operations where the critical current or towing speed was 1 knot for oil fences of about 1 m draft.

Figure 5 shows instantaneous velocity vector fields measured at random instants. From these, we can see the overall development of large-scale vortices in the shear layer separated from the fore fence. Quasi-periodic trains of vortices convecting down-stream are formed due to Kelvin–Helmholtz instability in the shear layer. For the case of a single fence in Fig. 5a, a large shear layer develops down-stream, and the vortical structure becomes stronger and larger through vortex pairing and merging processes as the flow progresses. In addition, the center of the shear layer moves downward from the initial region just behind the fore fence.

For a tandem fence with an open free surface (Fig. 5b), however, the development of a shear layer is not

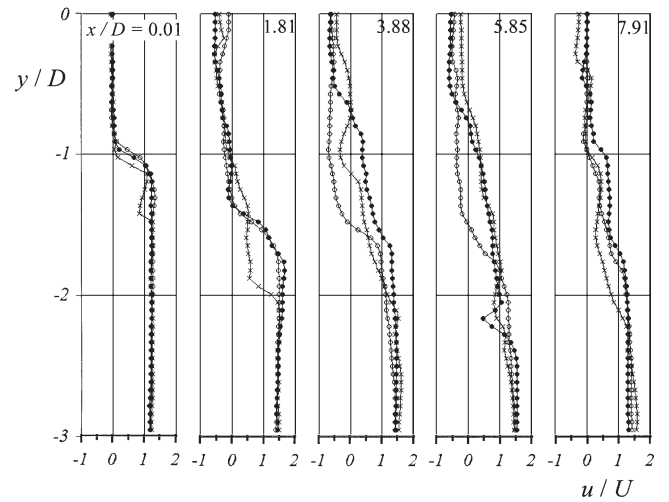


**Fig. 6.** Stream-wise velocity profiles for a single fence and a tandem fence of  $8D$  separation at  $Fr = 0.16$ . *Open circles*, open free surface (tandem); *solid circles*, closed free surface (tandem); *crosses*, single fence

strong in the rear half of the fluid zone between the two fences owing to the blockage effect of the aft fence. Some parts of the shear flow are entrained into the upper layer and cause a recirculating flow in an ascending and reverse direction, which interacts with the free surface. A large-scale counter-clockwise vortex is formed near the aft fence. The recirculating flow is faster than in the single fence case. Its interaction with the separated shear layer causes a wavy flow pattern in the shear layer and induces a relatively large horizontal negative velocity in the lower region.

For a tandem fence with a closed free surface (Fig. 5c), the development of a shear layer and a vortical structure are largely restricted. A shear layer develops in the initial region just behind the fore fence, and then moves upward and becomes almost flat in the rear half of the region. As the flow goes down-stream, it shows a flow structure which is similar to the wake behind a solid vertical fence. As shown in Fig. 5c, there is another small recirculating flow rotating counterclockwise just behind the fore fence near the free surface, in addition to the main recirculating flow. The different overall behavior of the shear layer, and especially of the large-scale vortex structures, has a significant influence on the entrainment process, and therefore on the entrainment of spilled oil.

The stream-wise velocity profiles at several longitudinal locations are shown in Fig. 6. With unsteady flow behavior between the tandem fences, which is mainly caused by the periodic vortices emanating from the fore-fence tip, it is very difficult to ascertain a repeatable time-averaged velocity field even with the PIV method. The PIV results shown in this article are the

compromised time-averaged values of about 50 instant images.

Since our major interest lies in the containment of oil slicks, attention should be focused on the flow behavior in the region  $|y/D| < 1$ . Throughout the experiment with the tandem fence, there were no visible disturbances on the free surface, except for an occasional capillary-type wave. Because of the low density of the oil, any oil which leaked below the fore fence would tend to float up to the free surface. Thus, if it is assumed that the oil layer covers the free surface between the tandem fences, even a capillary-wave disturbance may not exist owing to the viscous damping effect of the oil film.

It can be seen in Fig. 6 that despite the flat surface of the open free surface, there are noticeable differences in the velocity profiles of the open and closed free surfaces for the tandem fence. Just down-stream of the fore fence, the separating shear layer is very thin, and the velocity gradient in the  $y$ -direction is very steep near the shear-layer region, but as the flow goes down-stream, the shear layer expands and the velocity gradient decreases gradually. The stream-wise velocities with a tandem fence have appreciable negative values in the recirculating region of  $|y/D| < 1$ . Up to the location of  $x/D = 1.81$ , a tandem fence with either an open or a closed free surface produces a similar velocity profile. However, the velocity profiles in the middle region at  $x/D = 3.88$  and  $5.85$  are quite different. In this region, for the open free surface the stream-wise velocity has almost the same negative velocity down to the location of  $y/D = -1.5$ . The back flow in front of the rear fence is retarded as it approaches the fence owing to the presence of the aft fence. The flow retardation causes much larger streamline curvature than that for the backward-facing step flow.

### 5.2 Stream-wise velocity profiles

Figure 7 shows the velocity profiles obtained by computed results using the Navier–Stokes solver with a rigid free surface boundary condition, and also by the PIV method are shown for the three cases. The PIV results shown in Fig. 7a for a single fence are for an open free surface, while the computed results are for a closed free surface. The fact that these results agree fairly well means that at this Froude number, the effect of the free surface on the flow field around a single fence is not very significant.

Figure 7b shows the differences in the velocity profile between the computed and experimental results in the upper part of the middle region. The greater negative stream-wise velocity from the experimental results implies that the droplets are subject to a greater back-flow in this region. This, in turn, means that as the droplets or patches float up toward the surface they will be pushed

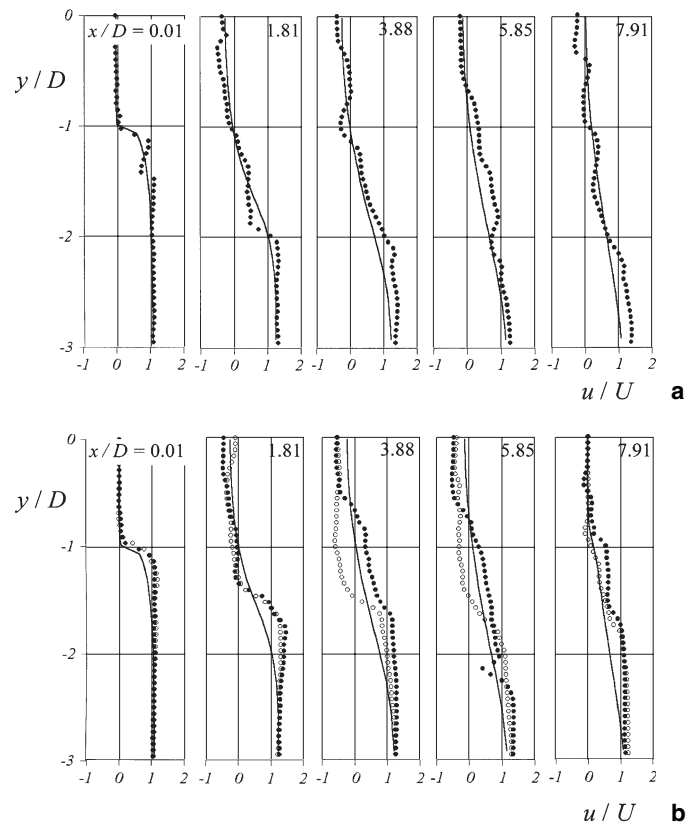


**Fig. 7.** Comparison of stream-wise velocity profiles obtained by computation and experiment. **a** Single fence: line, computed results; solid circles, PIV. **b** Tandem fence: line, computed results; open circles, open free surface; solid circles, closed free surface

toward the rear of the fore fence. This is a desirable condition, which enhances the oil containment between the tandem fences.

### 5.3 Droplet trajectory

Figure 8 shows the trajectories of a spherical paraffin ball of diameter 5 mm, which is intended to represent an oil droplet. The solid curve is the trajectory computed using Eq. 5, and the symbols show repeated experimental results. The particle release point  $(x_o, y_o)$  in Fig. 8a is  $(x_o/D, y_o/D) = (-2.0, -0.6)$ , and that in Fig. 8b is  $(-0.8, -0.6)$ . It can be seen that the trajectories obtained experimentally after the balls pass beneath the fence show inconsistent behavior behind the fence. The main reason is the unsteady nature of the tip vortex emanating from the tip of the fence. No attempt was made to obtain reasonable time-averaged trajectories from the experiment because of the impracticality of repeating the tests until a convergent time-averaged value could be obtained.

The back-flow behind the fore fence near the free surface shown in Fig. 7b is clearly demonstrated in Fig.

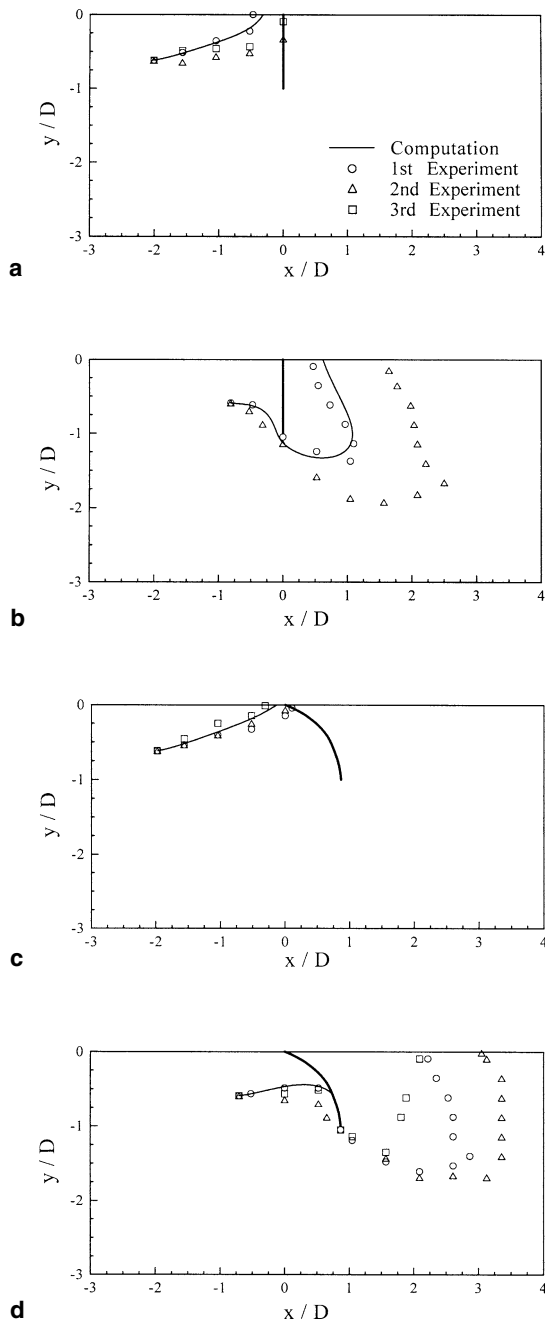


**Fig. 8.** Trajectories of paraffin balls around a vertical and a deflected fence for different initial release points at  $Fr = 0.29$ ,  $Re = 53100$ , and  $d_c = 5$  mm. **a**  $(x_o, y_o)/D = (-2, -0.6)$ ; **b**  $(x_o, y_o)/D = (-0.8, -0.6)$ ; **c**  $(x_o, y_o)/D = (-2, -0.6)$ ; **d**  $(x_o, y_o)/D = (-0.7, -0.6)$

8b, where the trajectory of the paraffin balls obtained experimentally, which is shown by the circular symbols, approaches closer to the back-side of the fore fence near the free surface. In Fig. 8b, the computed trajectory indicated by the solid curve has less back-flow velocity than the experimental results. This implies that the computed results should be considered as rather

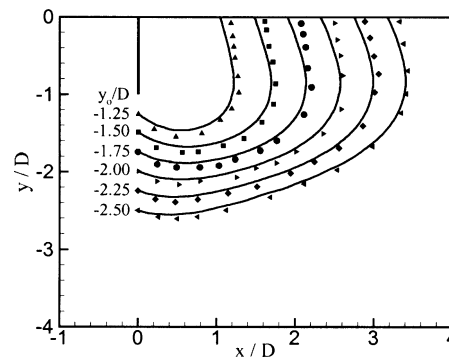


**Fig. 9.** Trajectories of oil droplets from different initial release points all directly below the fence at  $Fr = 0.22$  and  $d_c = 4.2$  mm. *lines*, computed results; *symbols*, experimental results

conservative when analyzing the effectiveness of the tandem fence.

From Fig. 8a and c, it can be seen that the droplet trajectories are reasonably well predicted by the computed results when the paraffin balls end their trajectories at the front face of the fence, but to trace the trajectories of the droplets all the way to the region at the back of the fence was found to be very difficult. The major reason is that the current computer code is not able to simulate the flow field disturbed by the periodic tip vortices with sufficient accuracy. However, if the initial release point is clearly designated directly below the fence, as shown in Fig. 9, the computed trajectories show excellent agreement with the measured ones. Since the sole purpose of using a tandem fence is to trap the oil slicks leaking under the fore fence, if computational Lagrangian tracking is satisfactory for the region between the two fences, the present computational method will be useful for assessing the effectiveness of a tandem fence.

Based on the analysis described above, it is concluded that the evaluation of the containment effectiveness of a set of tandem fences by flow-field computation based on the Navier–Stokes solver, with  $k-\epsilon$  turbulence modeling, a vanishing-velocity condition on the free surfaces, and the Lagrangian tracking method, is reasonable.

#### 5.4 Leakage lines

Figure 10 shows the leakage lines, which are defined as the demarcation lines dividing the fluid region into two zones. The zone below a leakage line (the leak zone) is the fluid region where an oil droplet released in this zone will leak below the fence, while an oil droplet released in the zone above (the trapping zone) will be trapped by the fore fence. These lines were obtained numerically by the Lagrangian tracking method. Figure 10a is for  $Fr = 0.116$  and Fig. 10b is for  $Fr = 0.232$ . The

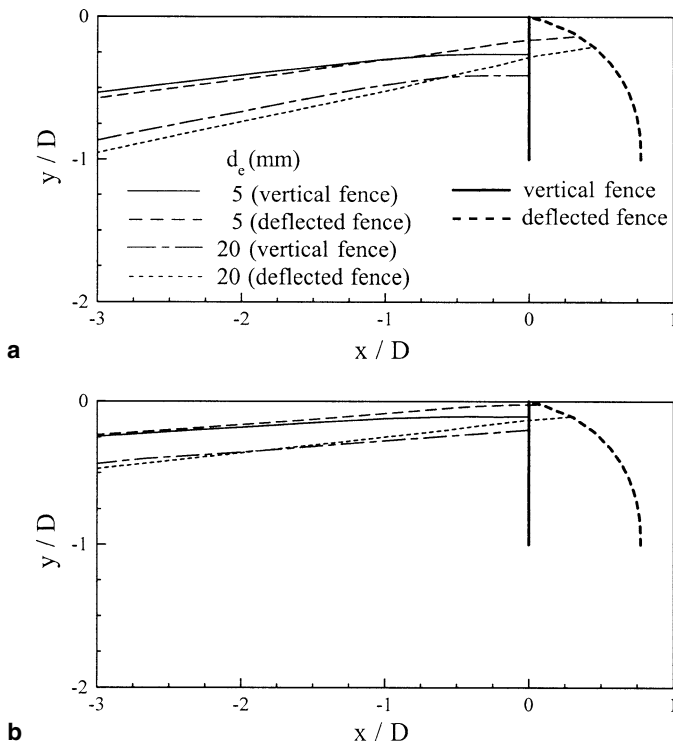


**Fig. 10.** Leakage lines for a vertical fence and a deflected fence for different oil droplet diameters and current speeds. **a**  $Fr = 0.116$ ; **b**  $Fr = 0.232$

different lines represent different sizes of oil droplet for the straight vertical fence and the fence which has been deflected (the dashed curve) by the current. (In a previous report by Lee et al.,<sup>7</sup> the relative effectiveness of a vertical or a deflectable fence was investigated.) As can be seen, a greater droplet size and a lower current speed definitely increase the trapping zone, while the deflected fence decreases the trapping zone near the fence. Thus, the leakage line indicates the approximate limit of the oil-layer thickness for an oil fence which can effectively contain spilled oil.

### 5.5 Droplet size

Figure 11 shows the computed trajectories of oil droplets of different diameters for  $Fr = 0.116$ . The diameter of an oil droplet is defined as  $d_e = (6V/\pi)^{1/3}$ . The release point is  $(0, -1.25D)$ , and the dotted curves are for the case when the skirt of the oil fence is deformed. As shown, the smaller the diameter of the oil droplet, the longer the trajectory. Thus, lumps of oil, which are more likely in real situations, would have more buoyancy than the single droplets investigated here, and would tend to float up closer to the back of the fore fence. Therefore, the trajectories of the bigger droplets may be a better representation of oil slicks escaping from the fore fence.

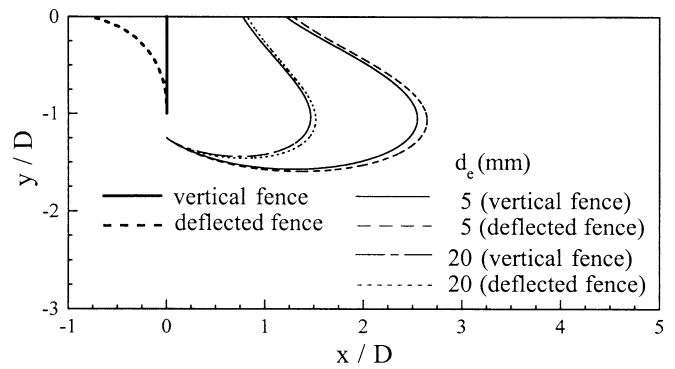


**Fig. 11.** Trajectories of oil droplets of different diameters behind a vertical fence and a deflected fence in a uniform current for a droplet release point at  $(0, -1.25D)$  at  $Fr = 0.116$

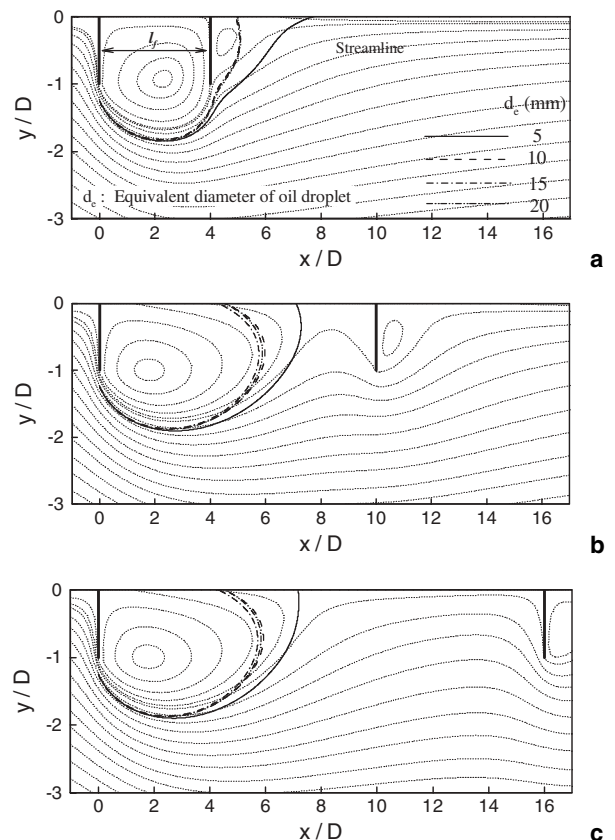


**Fig. 12.** Effect of the fence separation distance on the trajectories of oil droplets of various diameters at  $Fr = 0.232$ . Streamlines and velocity vectors for: **a**  $W = 4D$ ; **b**  $W = 10D$ ; **c**  $W = 16D$

### 5.6 Fence separation

Figure 12a shows the computed streamlines and velocity vectors for a tandem fence of  $W = 8D$  at  $Fr = 0.232$ , which corresponds to a full-scale current speed of 1.4 knots for a fence of 1 m draft. The reported leakage threshold velocity of the current is 1 knot. Thus, in this case,  $Fr = 0.232$  represents the current velocity beyond

the threshold velocity. This type of computation can be done for any other variations in current velocity ( $U$ ), different fence drafts ( $D_1$ ,  $D_2$ ), fence separation ( $W$ ), droplet size ( $d_e$ ), and water depth ( $H$ ), provided that the release point of the droplet is limited to the points directly underneath, or aft of, the fore fence tip.

Cho<sup>15</sup> found that a distance less than  $5D$  is no practical use for a tandem fence for  $U \geq 1$  knot. Thus, the minimum effective value of  $W$  is sought for  $W \geq 5D$ . Figure 12b and c show the droplet trajectories for  $d_e = 5$ , 10, and 15 mm at  $Fr = 0.232$ . These computed results, and the results of an experiment<sup>15</sup> with an initially contained oil layer between tandem fences of different separation distances, showed that  $W = 8D$  is the most effective not only for trapping oil slicks, but also for containing them for a long time for  $0.16 < Fr < 0.30$ . Therefore, our subsequent investigations were carried out for  $W = 8D$ .

### 5.7 Relative drafts of the fore and aft fences

Figure 13 shows the computed stream lines and trajectories for three different combinations of the drafts of

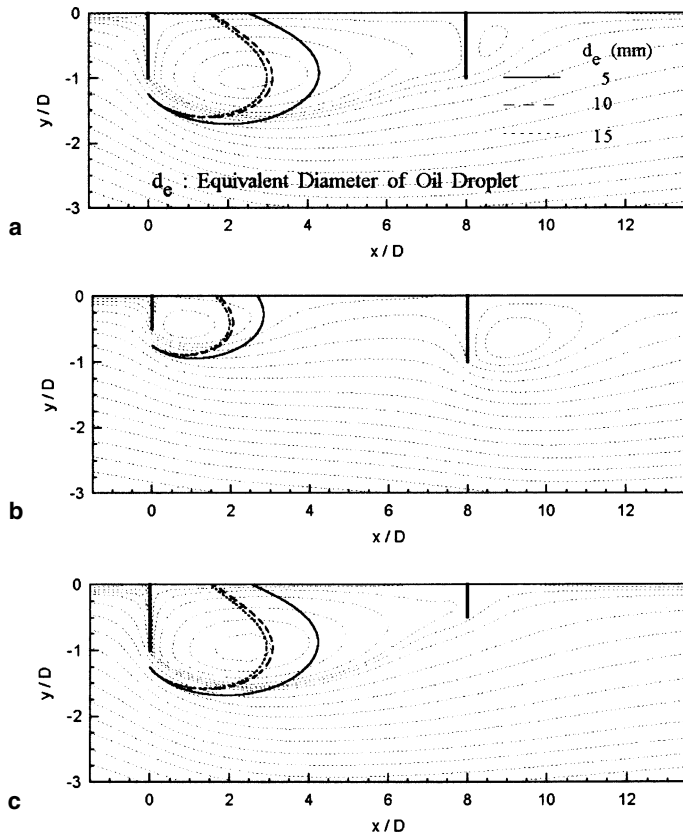


**Fig. 13.** Computed streamlines and trajectories of oil droplets released at  $(0, -1.25D)$  for a tandem fence of separation distance of  $8D$ , with different fore and rear drafts ( $D_1$ ,  $D_2$ ), at  $Fr = 0.232$ : **a**  $(D_1, D_2) = (D, D)$ ; **b**  $(D_1, D_2) = (D/2D)$ ; **c**  $(D_1, D_2) = (D, D/2)$

the fore and aft fences.  $D_1$  and  $D_2$  are the fore and aft draft, respectively. The trajectories for three different droplet diameters are shown. It seems obvious that once the oil slick leaks below the fore fence, the trapping of the oil is more effective for the case where  $D_1/D_2 = 0.5$ . However, by considering the higher possibility of a fore-fence leakage with the shallower draft, the conclusion is drawn that the case where  $D_1/D_2 = 1$  is the most effective.

### 5.8 Ratio of water depth to draft

In Fig. 14, the effect of the water depth in a shallow-water region on the effectiveness of the tandem fence is shown by tracing the trajectories of an oil droplet released at  $(0, -1.25D)$  for different water depths,  $H$ , at  $Fr = 0.232$ , and for identical fence drafts. For  $H = 15D$ , the result for the greater current speed ( $Fr = 0.464$ ) is also shown. The results show that the deeper the depth, the shorter the trajectory, and the greater the current speed, the longer the trajectory. The longer trajectory means a higher possibility of leakage below the aft fence. Thus, contrary to the expectation that the smaller the  $H/D$  ratio (up to 2) the greater the effectiveness at oil containment, the results show the opposite phenomenon.

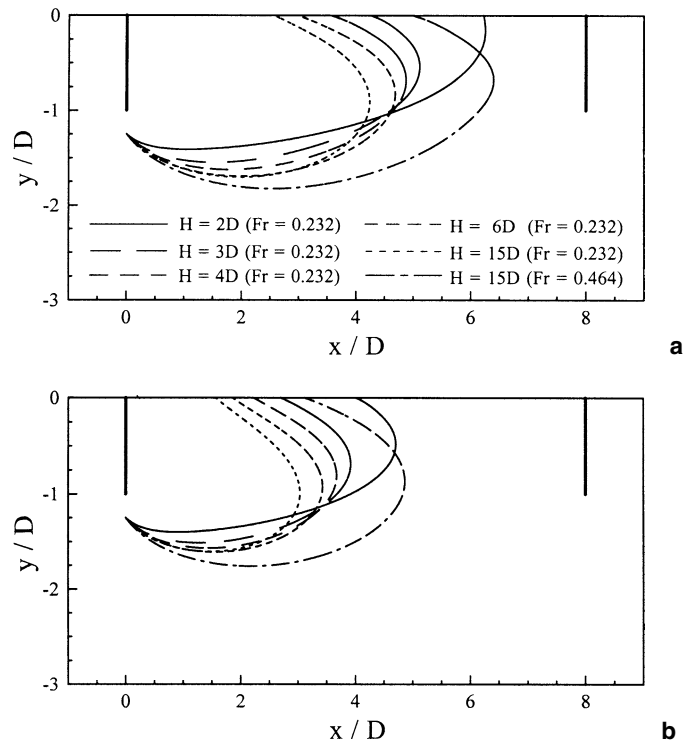


**Fig. 14.** Trajectories of oil droplets of two different equivalent diameters ( $d_e$ ) with a tandem fence of separation distance of  $8D$ , for various depths ( $H$ ), at  $Fr = 0.232$  and  $0.464$ , for a droplet release point at  $(0, -1.25D)$ . **a**  $d_e = 5$  mm; **b**  $d_e = 20$  mm

## 6 Conclusions

From the results of this investigation, the following conclusions can be drawn.

1. The flow-field computation using the Navier–Stokes solver with  $k$ - $\epsilon$  turbulence modeling and a rigid free-surface condition, together with the Lagrangian particle-tracking method, seems to be a reasonable tool to evaluate the effectiveness of a tandem fence.
2. The minimum fence separation distance was found to be about eight to ten times the fence draft.
3. An identical draft for both fences of a tandem fence seems to be more effective than other combinations of fore and aft fence drafts.
4. In a shallow-water region, the deployment of a tandem fence with a larger draft would not necessarily increase the effectiveness of oil-trapping. It is recommended that a gap is left between the fence tip and the bottom of the water which is more than twice the fence draft.

*Acknowledgments.* The authors express their appreciation for the support granted by the BK21 program of the Ministry of Education and Human Resources, and the Advanced Fluids Engineering Research Center of Pohang University of Science and Technology. They also acknowledge the assistance of their former and present graduate students N.S. Cho, M.S. Koh, and S.K. Chung in carrying out some of the experiments.

## References

1. Comrack D (1983) Response to oil and chemical marine pollution. Applied Science Publishers, New York
2. Delvigne GAL (1987) Laboratory experiments on oil spill protection of a water intake. In: Vandermulen JH, Hurdey SE (eds) Oil in fresh water: chemistry, biology, countermeasure technology. Pergamon, Oxford, pp 446–458
3. Lo JM (1996) Laboratory investigation of single floating booms and series of booms in the prevention of oil slick and jellyfish movement. Ocean Eng 23:519–531
4. Lee CM, Kang KH, Cho NS (1998) Trapping of leaked oil with tandem oil fences with Lagrangian analysis of oil droplet motion. J OMAE, ASME Trans 120:519–531
5. Kang KH, Lee CM (1995) On the threshold leakage velocity of oil under an oil fence. Proceedings MARIENV '95, Tokyo, vol 2, pp 974–981
6. Lee CM, Kang KH (1997) Prediction of oil boom performance in currents and waves. Spill Sci Tech Bull 4:257–266
7. Lee CM, Kang KH, Han DG (1998) On the oil-fence deflection and behavior of the oil–water interface between tandem fences. AFERC Report, Pohang University of Science and Technology, AFR-97-CE, pp 3–35
8. Lee CM, Lee SJ, Kim YG (2001) Investigation of the effectiveness of tandem oil fences under currents. Proceedings OMAE'01, OMAE01/OSU-5031 (on CD-ROM), Rio de Janeiro, pp 1–8
9. Han DG, Lee CM, Lee SJ (2001) Flow behavior around tandem oil fences. Proceedings PRADS 2001, Shanghai. Elsevier, vol 1, pp 451–457
10. Maxey MR, Riley JJ (1983) Equation of motion for a small rigid sphere in a nonuniform flow. Phys Fluids 26:883–889
11. Berlement A, Desjonqueres P, Gouesbet G (1990) Particle Lagrangian simulation in turbulent flows. Int J Multiphase Flow 16:19–34
12. Clift R, Grace JR, Weber ME (1978) Bubbles, drops, and particles. Academic Press, New York
13. Jones WP, Launder BE (1972) The prediction of laminarization with a two-equation model of turbulence. Int J Heat Mass Transfer 15:301–314
14. Shin DS, Choi JH, Lee SJ (2000) Velocity-field measurement of flow inside the snout of a continuous hot-dip galvanizing process using a single-frame PIV technique. Iron Steel Inst Jpn J 40: 484–490
15. Cho NS (1997) Lagrangian analysis of oil droplet motion around oil fences (in Korean). Masters Thesis, Department of Mechanical Engineering, Pohang University of Science and Technology, p 76